論文 / 著書情報
Article / Book Information

Title	Study of air-suspended RF MEMS inductorconfigurations for realizing large inductancevariations
Author	Yutaka Mizuochi, Shuhei Amakawa, Noboru Ishihara, Kazuya Masu
Journal/Book name	Proceedings of the Argentine School of Micro-Nanoelectronics, Technology and Applications 2009, , , pp. 50-55
発行日 / Issue date	2009, 10
権利情報 / Copyright	(c)2009 IEEE. Personal use of this material is permitted. However, permission to reprint/republish this material for advertising or promotional purposes or for creating new collective works for resale or redistribution to servers or lists, or to reuse any copyrighted component of this work in other works must be obtained from the IEEE.

Study of air-suspended RF MEMS inductor configurations for realizing large inductance variations

Yutaka Mizuochi, Shuhei Amakawa, Noboru Ishihara, and Kazuya Masu
Integrated Research Institute, Tokyo Institute of Technology
4259-R2-17 Nagatsuta, Midori-ku, Yokohama 226-8503, Japan
Tel: +81-45-924-5031, Fax: +81-45-924-5166, E-mail: paper@lsi.pi.titech.ac.jp

***Abstract*—The configurations of the following three types of high-Q air-suspended RF MEMS inductors (in particular, their potentials) are studied to identify the configuration that would yield large inductance variations: an inductor with two angularly meandered lines, a spiral inductor with patterned shields of different areas, and a spiral inductor with metallic frames of different sizes. The potentials of MEMS inductors fabricated on high-resistivity Si substrates are experimentally determined. The inductance of the spiral inductors changes by at most 23% when the shield area or the frame size in the inductors is changed. On the other hand, the inductance of the meander-type inductor changes by 108% (from 2.65 nH to 5.50 nH) because of the large change in the current loop area. The configuration of the meander-type inductor is thus considered suitable for realizing an RF MEMS variable inductor with large inductance variations.**

I. Introduction

Currently, a number of wireless services such as mobile phones, LANs, and televisions are being used, and more such services are expected to be developed in the near future. One-chip RF LSI system solution is desired for lowering cost of terminals supporting multiple wireless services. In particular, multi-band and wide-band RF circuit technologies that cover a wide frequency range of, say, 0.8 to 6 GHz is required. Conventionally, variable capacitors have been used in LC circuits for frequency tuning. However, the frequency range that can be covered by varying C alone is limited. Therefore, tunable inductors with a high Q and wide tuning range are desired for multiband and wideband RF LSI systems.

Several methods have been proposed for designing tunable inductors with a wide inductance range and high Q-factor. The simplest method for varying the inductance involves the use of switches [1], [2]. [1] used series-connected inductors and varied the inductance by shunting some of the inductors with the help of switches. While the inductance tuning range, defined by $(L_{\max} - L_{\min})/L_{\min}$, was more than 100%, the Q factor was less than 5 because of the significant ohmic loss introduced by the switches. In [2], the primary inductor has a couple of magnetically-coupled auxiliary inductors with shunt switches. The inductance variation in this case was limited to 25%.

Other inductor configurations without switches have also been reported [3]–[6]. In [3], inductance variation was attempted by deforming a spiral inductor. However, in this case, the observed inductance variation was only 3%. According to [4], [5], the separation between parallel-connected inductors is controlled by temperature. The maximum inductance variation obtained with these inductors is 18% [4]. The inductor in [6] comprised a spiral inductor with a metal shield above it. An inductance variation of 38% was observed when the separation between the inductors was changed.

In this research, the configuration of an air-suspended RF MEMS inductor that is ideal for realizing large inductance variations is determined by investigating three possible inductor configurations. The rest of this paper is organized as follows. In section II, the configurations of three variable inductors are discussed. In section III, the measurement results are presented. Section IV shows the comparison between the results obtained with the three inductor configurations. Section V includes concluding remarks.

II. Variable inductor configurations

In this section, we discuss three variable inductor configurations.

A. Meander-type inductor with varying current loop areas

The self-inductance L of a current loop is given by

$$L = \frac{1}{I}\iint_S \boldsymbol{B}\cdot \mathrm{d}\boldsymbol{S} \tag{1}$$

$$= \frac{1}{I}\oint_C \boldsymbol{A}\cdot \mathrm{d}\boldsymbol{l} \tag{2}$$

$$= \frac{\mu}{4\pi}\oint_C\oint_C \frac{\mathrm{d}\boldsymbol{l}\cdot \mathrm{d}\boldsymbol{l}'}{r}, \tag{3}$$

where I is the loop current; $\boldsymbol{B} = \nabla\times\boldsymbol{A}$, the magnetic flux density induced by I; $\boldsymbol{A}$, the vector potential; and S, the surface enclosed by the loop C. $\mathrm{d}\boldsymbol{l}$ and $\mathrm{d}\boldsymbol{l}'$ are the vector differentials on C. r is the distance between $\mathrm{d}\boldsymbol{l}$ and $\mathrm{d}\boldsymbol{l}'$. From this equation, it is apparent that L is proportional to the loop area S and the magnetic permeability μ. If the number of loops is n, L would be proportional to n^2.

$$L \propto S\cdot\mu\cdot n^2. \tag{4}$$

The total L value is mostly determined by the abovementioned three factors. If the current loop area can be controlled, L can be varied efficiently.

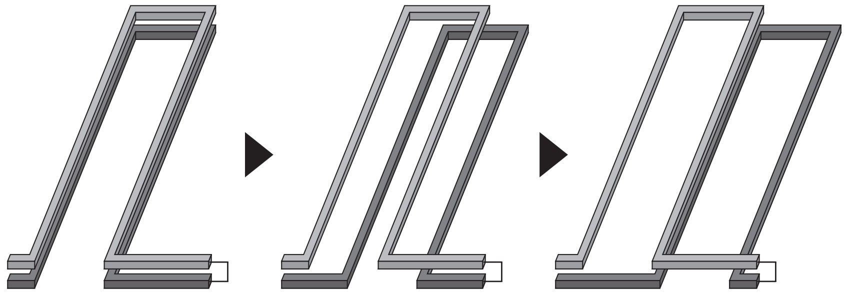

Fig. 1. Meander-type inductors with different loop areas.

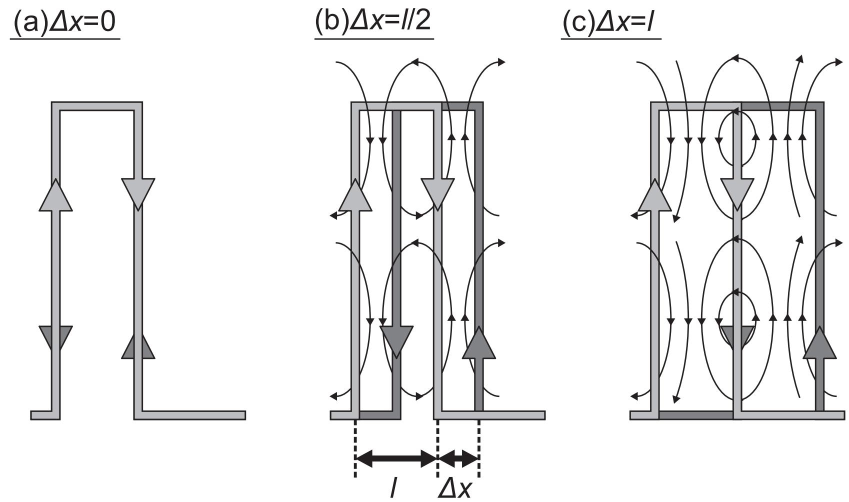

Fig. 2. Relation between current loop area and magnetic flux.

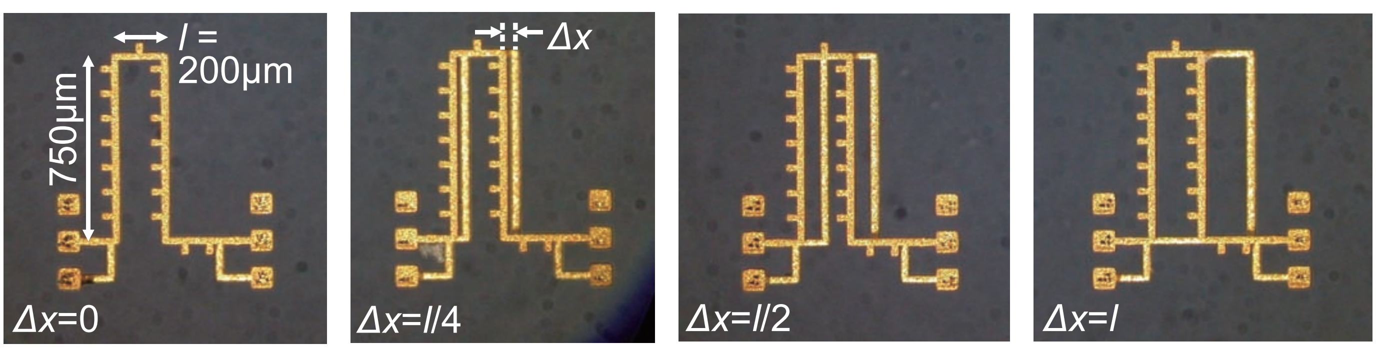

Fig. 3. Micrographs of fabricated meander-type inductors. The length of each wire (excluding the pads and leads) is 2 mm. $l = 200\,\mu$m.

Fig. 1 shows the proposed meander-type inductors with different loop areas. One inductor consists of two angularly meandered wires that are to be shorted at, say, the right-hand end. The current loop area can be changed by the relative displacement of the two meandered wires. Fig. 2 shows the mechanism underlying the inductance variation. Thick arrows on wires and thin black arrows show current and magnetic flux, respectively. In case (a), where $\Delta x = 0$, the current loop area is very small because one wire is positioned exactly above the other. In case (b), where $\Delta x = l/2$, two current loops with a width of Δx are formed, and the inductance is expected to increase. In case (c),where $\Delta x = l$, the current loop area is maximized, and consequently, the inductance is expected to assume a maximum value. The "comb-drive [7]" is a MEMS actuator that could be used to implement a meander-type variable inductor.

To confirm the effect of the current loop area on the inductance, air-suspended MEMS inductors, shown in Fig. 3, were designed and fabricated. Fig. 4 shows a bird's-eye view of one of the fabricated inductors. The dependence of inductance on the current loop area can be determined by studying these test inductors. Two sets of inductors were fabricated: one set with a wire length of 2 mm, and the other set with a wire length of 4 mm. Each inductor consists of two such meandered wires.

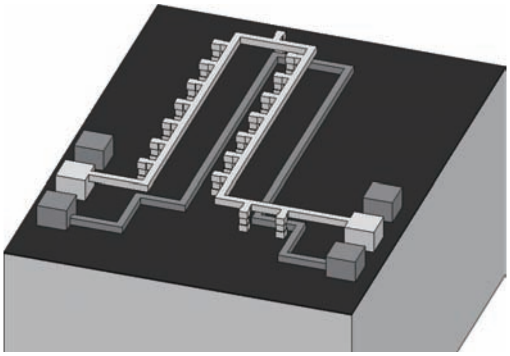

Fig. 4. Bird's-eye view of a meander-type inductor.

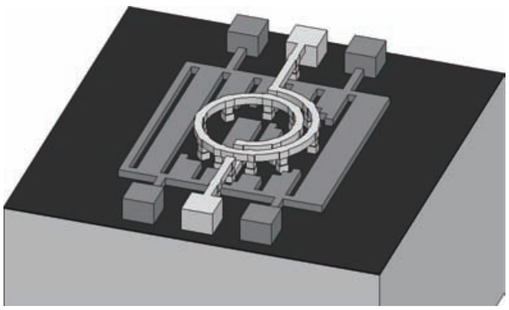

Fig. 6. Bird's-eye view of a spiral inductor with patterned shields.

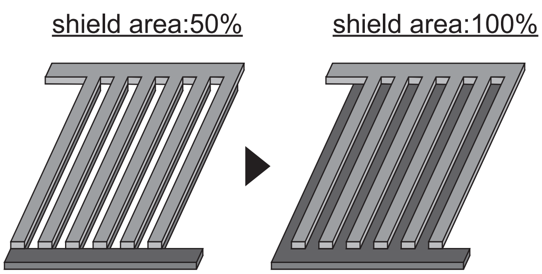

Fig. 7. A possible method of changing the shield area. The area changes with the relative displacement of the two comb-shaped shields.

Fig. 3 shows the micrographs of the inductors with 2-mm-long wires.

B. Spiral inductor with varying shield areas

Fig. 5 shows the fabricated spiral inductors with patterned shields, and Fig. 6 shows a bird's-eye view of one such inductor. The mutual inductances between the spiral inductor and the shields changed with the shield area. Three inductors with different shield areas were fabricated, and a situation in which the shield area could be controlled by using two movable comb-shaped patterns was simulated, as shown in Fig. 7.

C. Spiral inductor with varying metallic frame sizes

Fig. 8 shows spiral inductors with different frame sizes, and Fig. 9 shows a bird's-eye view of one such inductor. The frame serves as the current return path. The leftmost inductor in Fig. 8 has the smallest loop area, while the rightmost one has the largest loop area. The inductance is expected to change according to (2).

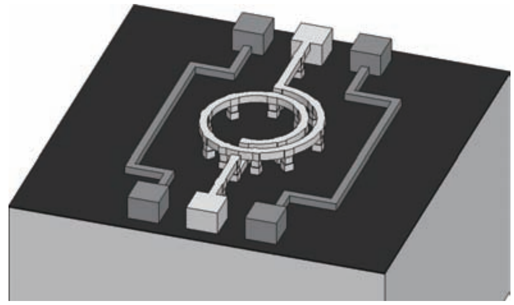

Fig. 9. Bird's-eye view of a spiral inductor with a frame.

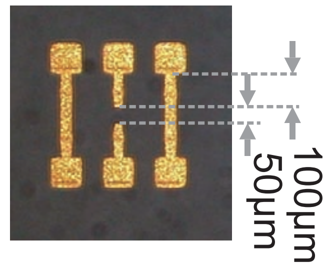

Fig. 10. Open pattern used for de-embedding.

III. Measurement results

Two-port S-parameters of the fabricated test inductors were measured by using a vector network analyzer. The inductance L and the quality factor Q were calculated from the following equations.

$$L = \frac{1}{2\pi f}\mathrm{Im}\left(\frac{1}{Y_{11}^{\mathrm{ind}}}\right), \tag{5}$$

$$Q = -\frac{\mathrm{Im}\left(\frac{1}{Y_{11}^{\mathrm{ind}}}\right)}{\mathrm{Re}\left(\frac{1}{Y_{11}^{\mathrm{ind}}}\right)}, \tag{6}$$

where $\boldsymbol{Y}^{\mathrm{ind}}$ is the two-port admittance matrix of the de-embedded inductor. De-embedding was performed by using the formula

$$\boldsymbol{Y}^{\mathrm{ind}} = \boldsymbol{Y}^{\mathrm{meas}} - \boldsymbol{Y}^{\mathrm{open}}, \tag{7}$$

where $\boldsymbol{Y}^{\mathrm{meas}}$ and $\boldsymbol{Y}^{\mathrm{open}}$ are the admittance matrices of the measured device and the open pattern shown in Fig. 10, respectively.

All the test inductors were fabricated on a Si wafer with a 3-μm-thick surface oxide layer. The resistivity of the wafer was $1\,\mathrm{k}\Omega\cdot\mathrm{cm}$. A two-metal-layer process was used for this purpose, and the metal used was gold. The thickness of each metal layer was $20\,\mu$m and each line width was $20\,\mu$m.

A. Dependence of inductance on loop area in meander-type inductor

Fig. 11 and Fig. 12 show the measured L and Q, respectively. In the case of inductors consisting of a pair of 2-mm-long wires, L at 100 MHz increased from 1.54 nH to 2.79 nH

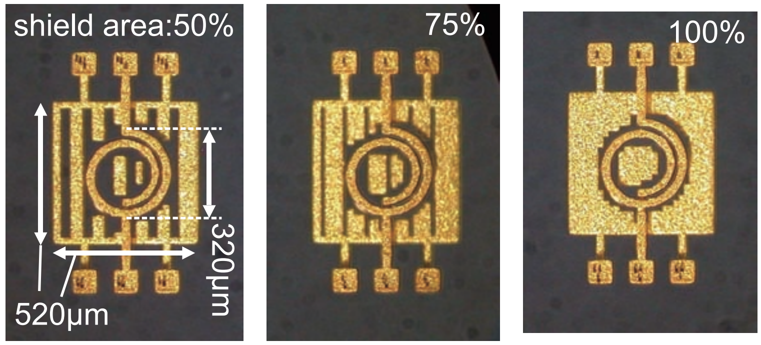

Fig. 5. Micrographs of fabricated spiral inductors with different shield areas.

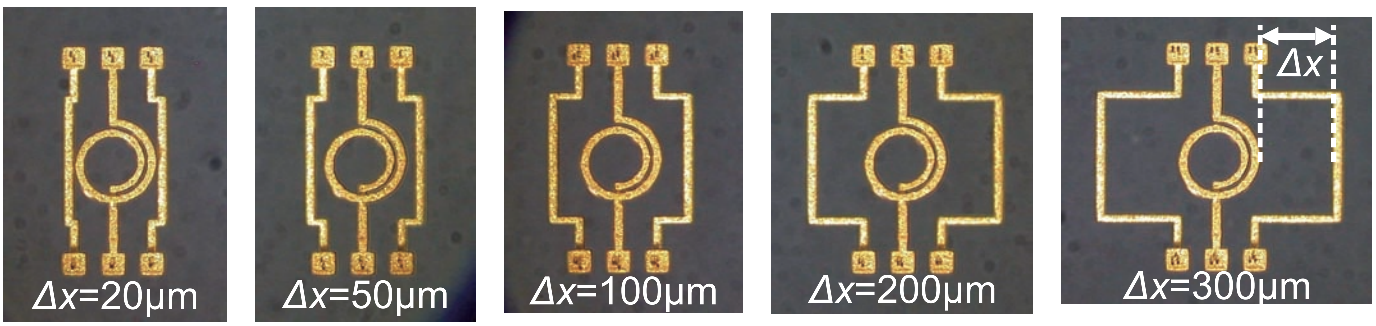

Fig. 8. Micrographs of the fabricated spiral inductors with different frame sizes.

when Δx was changed from $0\,\mu$m to $200\,\mu\mathrm{m}\,(=l)$, as shown in Fig. 11. In the case of inductors with 4-mm-long wires, L increased from 2.65 nH to 5.50 nH, as shown in Fig. 12. Note that the value of L at 100 MHz should be close to the intrinsic inductance of the device, whereas at higher frequencies, the L value becomes larger due to the presence of parasitic parallel capacitance. The variations in L were 81% and 108%, and the maximum Q-factors were 19 and 17, respectively.

B. Dependence of inductance on shield area in spiral inductor

The frequency dependences of the measured L and Q are shown in Fig. 13. The inductance can be varied by changing the area of the shield. Wideband high-Q characteristics were obtained when the shield area was fixed. Further, L at 100 MHz decreased from 1.12 nH to 0.97 nH when the shield area was increased by 50% to 100%. The variation in L was 15%, and the maximum Q-factor was 37.

C. Dependence of inductance on frame size in spiral inductor

L can be varied by changing the frame size, as shown in Fig. 14. At 100 MHz, L increased from 1.16 nH to 1.42 nH when the frame size was changed from $\Delta x = 20\,\mu$m to $300\,\mu$m. The variation in L was 23%, and the maximum Q-factor was 38.

IV. Discussion

The measured L values for all the test inductors are summarized in Fig. 15. Fig. 15(a) shows the maximum and minimum values of L at 100 MHz. Fig. 15(b) shows the dependence of L at 100 MHz on the relative displacement of the two meandered wires (Fig. 3), shield pattern area (Fig. 5), and frame size (Fig. 8). Apparently, the inductance of the meander-type inductor can be varied most effectively because with this configuration, the self-inductance can be controlled directly by changing the current loop area. The Q-factor also increases concurrently with L because the increase in L does not affect the resistive loss in the wires.

In the case of the spiral inductor with a controlled shield area (Fig. 5), the mutual inductances between the spiral and the shield patterns could be controlled. In this case, both L and the Q-factor decreased with an increase in the shield area. The inductance variation was approximately 15%.

In the spiral inductor in which the frame size was controlled (Fig. 8), the loop area changed in the same manner as in the case of the meander-type inductor. However, in this case, the main contribution to the inductance came from the spiral part. Because of this, the inductance variation was not as significant as in the case of the meander-type inductor.

The maximum Q-factor of the meander-type inductors was less than 20, while that of the spiral inductors with metal shields was higher. The low Q of the meander-type inductors can be attributed to the high resistive loss in the relatively long wires used in these inductors.

V. Conclusion

Herein, air-suspended RF MEMS inductor configurations suitable for achieving large inductance variations are studied, and the following conclusions are drawn from our experimental results.

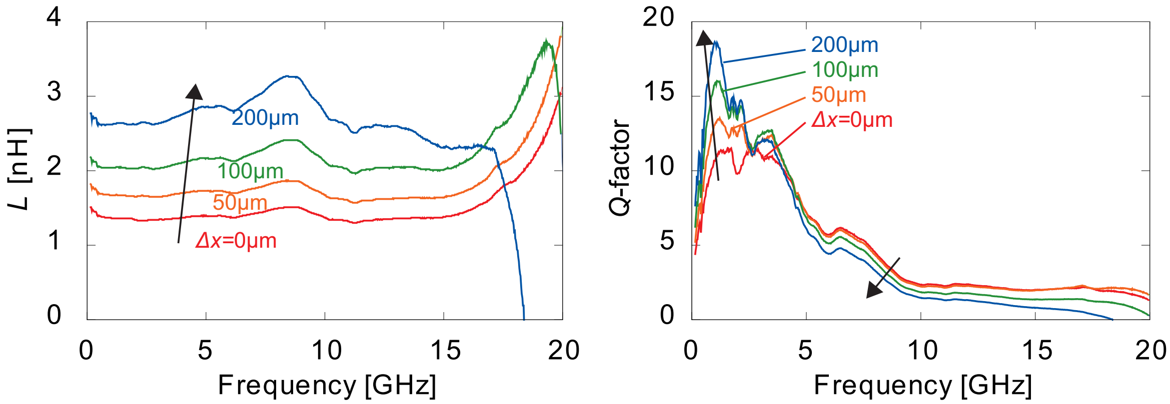

Fig. 11. L and Q-factor of meander-type inductors with 2-mm-long wires. $\Delta x = 0,\ 50,\ 100$, and $200\,\mu$m.

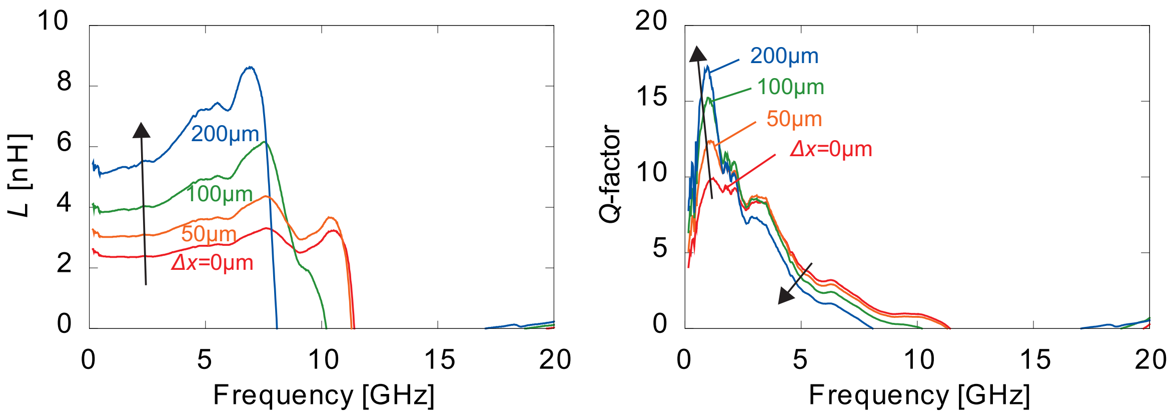

Fig. 12. L and Q-factor of meander-type inductors with 4-mm-long wires. $\Delta x = 0,\ 50,\ 100$, and $200\,\mu$m.

1) The meander-type inductor configuration (Fig. 1) is suitable for achieving large inductance variations.
2) The inductances of the fabricated meander-type inductors range from 2.65 nH to 5.50 nH; in other words, the inductance variation is 108%.
3) The inductance can also be varied by controlling the shield area (Fig. 5) or the size of the metallic frame (Fig. 8). However, the inductance variation achieved with these methods is not as good as that achieved with the meander-type inductor.
4) Air-suspended MEMS inductors are superior to on-chip inductors owing to their wideband high-Q characteristics, and hence, they are suitable for use in wide- and multiband RF systems.

In this study, we concentrated on clarifying the configuration suitable for achieving large inductance variations. The very important question of how to actually realize mechanically or electronically variable inductors shall be addressed elsewhere.

Acknowledgment

This study was partially supported by NEDO, KAKENHI, STARC, MIC.SCOPE, and VDEC in collaboration with Agilent Technologies and Cadence Design Systems, Inc.

References

[1] P. Park, C. S. Kim, M. Y. Park, S. D. Kim, and H. K. Yu, “Variable inductance multilayer inductor with MOSFET switch control,” *IEEE Electron Device Letters*, vol. 25, no. 3, pp. 144–146, Mar. 2004.

[2] M. Rais-Zadeh, P. A. Kohl, and F. Ayazi “MEMS switched tunable inductors,” *IEEE Journal of Microelectromechanical Systems*, vol. 17, no. 1, pp. 78–84, Feb. 2008.

[3] Y. Yokoyama, T. Fukushige, S. Hata, K. Masu, and A. Shimokohbe “On-chip variable inductor using microelectromechanical systems technology,” *Japanese Journal of Applied Physics*, vol. 42, no. 4B, pp. 2190–2192, Apr. 2003.

[4] V. M. Lubecke, B. Barder, E. Chan, D. Lopez, M. E. Cross, and P. Gammel, “Self-assembling MEMS variable and fixed RF inductors,” *IEEE Transactions on Microwave Theory and Techniques*, vol. 49, no. 11, pp. 2093–2098, Nov. 2001.

[5] I. Zine-El-Abidine, M. Okoniewski, and J. G. McRory, “A new class of tunable RF MEMS inductors,” *International Conference on MEMS, NANO and Smart Systems*, pp. 114–115, Jul. 2003.

[6] H. Sugawara, Y. Yoshihara, H. Ito, K. Okada, and K. Masu, “Wide-range RF variable inductor on Si CMOS chip with MEMS actuator,” *IEEE European Microwave Conference*, pp. 701–704, Oct. 2004.

[7] W. C. Tang, M. G. Lim, and R. T. Howe, “Electrostatic comb drive levitation and control method,” *IEEE Journal of Microelectromechanical Systems*, vol. 1, no. 4, pp. 170–178, Dec. 1992.

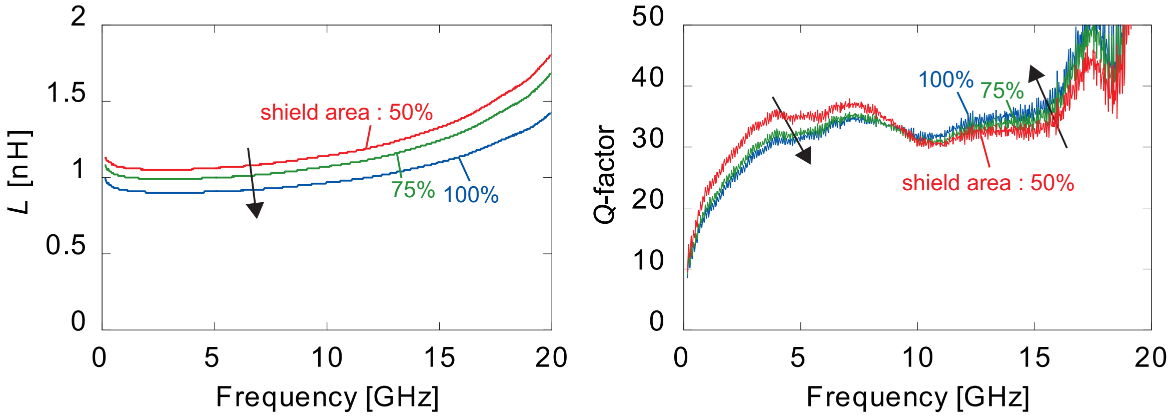

Fig. 13. L and Q-factor of spiral inductors with patterned shields. The shield areas are 50%, 75%, and 100%.

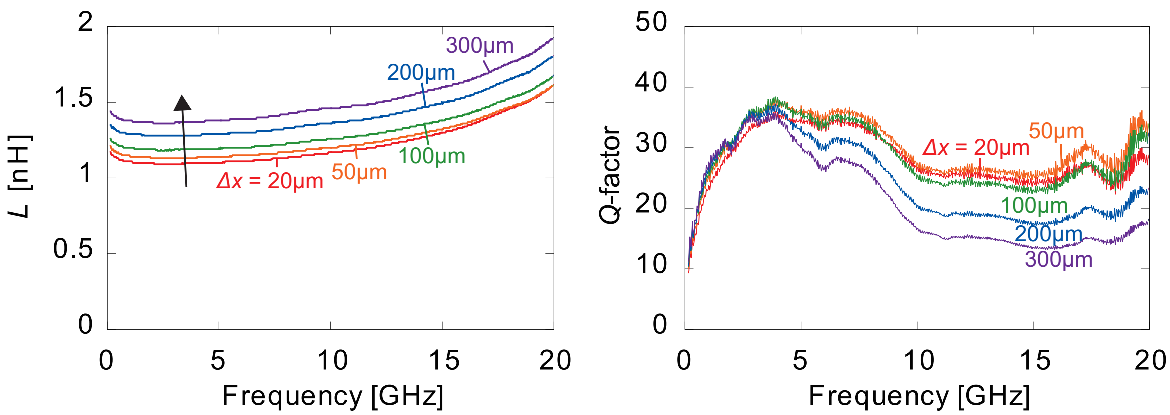

Fig. 14. L and Q-factor of spiral inductors with different frame sizes. $\Delta x = 20,\ 50,\ 100,\ 200,$ and $300\,\mu$m.

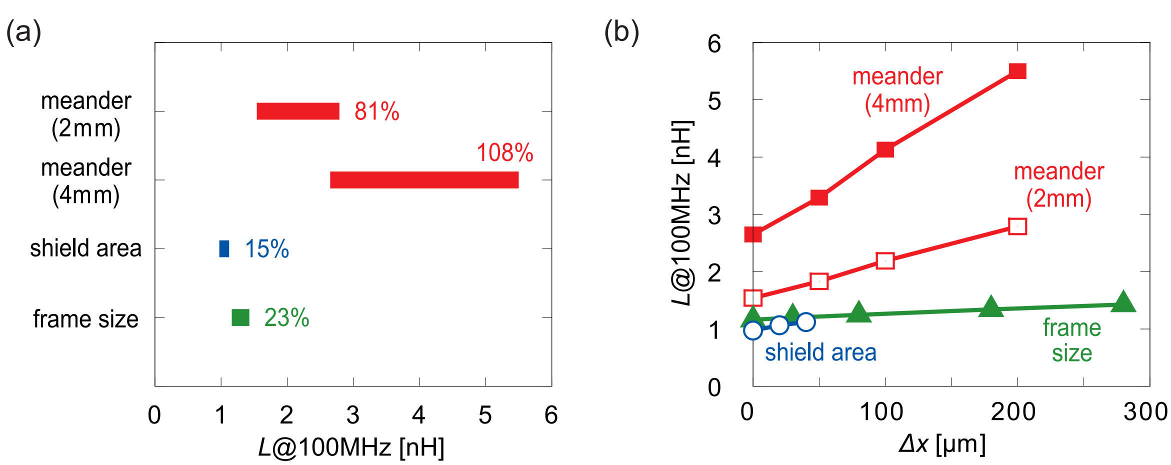

Fig. 15. Summary of all test inductors. (a) The maximum and minimum values of L at 100 MHz. (b) Dependence of L at 100 MHz on the shield area or length of the wire slide.